Removal of As(V) from wastewaters using magnetic iron oxides formed by zero-valent iron electrocoagulation

Yi Wang[a], Lihu Liu[a], Xiong Yang[a], Steven L. Suib[b], Guohong Qiu[a,*]

[a] Key Laboratory of Arable Land Conservation (Middle and Lower Reaches of Yangtse River), Ministry of Agriculture, Hubei Key Laboratory of Soil Environment and Pollution Remediation, College of Resources and Environment, Huazhong Agricultural University, Wuhan 430070, Hubei Province, China

[b] Department of Chemistry, University of Connecticut, 55 North Eagleville Road, Storrs, Connecticut 06269-3060, United States

* Corresponding author: Qiu GH, qiugh@mail.hzau.edu.cn

Abstract

Electrocoagulation of zero-valent iron has been widely applied to the removal of dissolved arsenic, but the solid-liquid separation of arsenic-containing precipitates remains technically challenging. In this work, zero-valent iron was electrochemically oxidized to magnetic iron oxides for the removal of As(V) from simulated and actual mining wastewaters. The results indicated that lepidocrocite was formed when zero-valent iron was oxidized by dissolved oxygen, but ferrihydrite and green rust were first formed and then transformed to magnetic iron oxides (mainly magnetite and maghemite) in the electrochemical oxidation from 0 to 0.9 V (*vs*. SCE), which facilitates the adsorption of As(V) and subsequent solid-liquid separation under a magnetic field. In simulated As(V)-containing solution with initial pH 7.0, zero-valent iron was electrochemically oxidized to magnetite and maghemite at 0.6 V (*vs*. SCE) for 2 h. The As(V) concentration first decreased from

5127.5 to 26.8 μg L^{-1} with a removal ratio of 99.5%. In actual mining wastewaters, zero-valent iron was electrochemically oxidized to maghemite at 0.6 V (*vs*. SCE) for 24 h, and the As(V) concentration decreased from 5486.4 to 3.6 μg L^{-1} with a removal ratio of 99.9%. The removal ratio of As(V) increased slightly with increasing potential, and increased first and then decreased with increasing initial pH. Compared with that of SO_4^{2-} and NO_3^-, the presence of Cl^- significantly enhanced the removal of As(V). This work provides a highly efficient, facile and low-cost technique for the treatment of arsenic-containing wastewaters.

Keywords: Arsenic, Electrocoagulation, Zero-valent iron, Magnetic iron oxides, Wastewater

1. Introduction

The environmental behaviors and removal technologies of arsenic (As) have been extensively studied due to high toxicity and carcinogenicity. Arsenic pollution in waters has been further aggravated by weathering of arsenic-bearing minerals, discharge of mining and metallurgical wastewaters and abuse of organic arsenic pesticides (Aredes et al., 2013; He et al., 2018). As-contaminated groundwater has posed serious threats to the health of people in China, India and Bangladesh (Chowdhury et al., 2000; Zhang et al., 2017). The World Health Organization recommends that the maximum As concentration should not exceed 10 μg L^{-1} in drinking water (Edition, 2011). The Chinese national standard system (GB30770-2014) stipulates that the As concentration in mining wastewaters should be lower than 100 μg L^{-1}. Therefore, it is imminent to develop highly efficient and more appropriate As-removal technologies for the treatment of polluted waters. Dissolved As mainly exists as arsenate [As(V)] or arsenite [As(III)] in waters depending on

the redox potential (Eh) and pH (Gong et al., 2002). As(V) is stable under aerobic or oxidative conditions, while As(III) is stable under anaerobic or mild reduction conditions (Choong et al., 2007). It is a common practice to oxidize As(III) to As(V) through certain techniques prior to removal from watewaters (Singh et al., 2015). Therefore, research on the removal of As(V) from wastewaters in open environments is of great practical significance.

For As removal, various methods have been developed, including chemical coagulation, membrane filtration, ion exchange and adsorption (Mondal et al., 2006; Mondal et al., 2013; Song et al., 2017), and chemical coagulation has also been widely applied to wastewater treatment. Dissolved As tends to be adsorbed or co-precipitated in the presence of coagulants including zero-valent iron, iron salts and aluminum salts, which can facilitate the further separation of As (Eljamal et al., 2013; Lakshmanan et al., 2010). Both zero-valent iron and nanoscale zero-valent iron have good performance in As removal from wastewater. However, compared with nanoscale zero-valent iron, zero-valent iron can be widely used due to its lower cost and degree of aggregation (Fu et al., 2014). As(V) is removed through surface adsorption and co-precipitation with Fe(III) on zero-valent iron, while As(III) is removed by direct adsorption on zero-valent iron or first oxidized to As(V) and then adsorbed on the surface (Eljamal et al., 2011; Eljamal et al., 2011). However, it is very challenging to appropriately control the dosage of coagulants in the chemical coagulation process, and a significant decrease in pH is not conducive to the adsorption and removal of As (Lacasa et al., 2013). Compared with chemical coagulation, electrocoagulation has a different way of providing coagulants to the system. Electrocoagulation involves the simple electrochemical oxidation of anode materials (usually iron or aluminum) with the in-situ production of coagulants, without the addition of any other chemical substances (Hakizimana et al., 2017).

When zero-valent iron is used in electrocoagulation, aqueous Fe^{2+} ions are formed and part of Fe^{2+} ions are oxidized to form Fe^{3+}. They are released into the bulk solution to generate Fe(III) (hydr)oxides for the effective adsorption and removal of As (Lakshmanan et al., 2009; Wan et al., 2011). In addition, it is not necessary to adjust the pH and chemicals in the electrocoagulation process, which greatly simplifies the operation process and reduces the cost (Lakshmanan et al., 2010; Mondal et al., 2006; Ungureanu et al., 2015).

It remains technically challenging to achieve highly efficient separation and recovery of As-containing precipitate, which can significantly reduce secondary pollution and are of great significance for the sustainability of the electrocoagulation process (Alka et al., 2020; Nidheesh and Singh, 2017). At present, the recovery of As-containing flocs is mainly conducted through filtering and flocculation with alum by taking advantage of gravity (Kobya et al., 2020; Thakur et al., 2019). Environment-friendly magnetic iron oxides, including magnetite (Fe_3O_4) and maghemite (γ-Fe_2O_3), are widely used for As adsorption and recovery due to their recyclability and stability (Su, 2017; Tuutijärvi et al., 2009). They can efficiently adsorb As and solid-liquid separation can be easily realized under magnetic fields, which is more convenient than conventional filtration and centrifugal separation (Siddiqui and Chaudhry, 2017).

With respect to the As adsorption reaction, magnetic iron oxides can be produced in many ways. Magnetite can be prepared as slurry first, and then transferred to the reaction system, and magnetic iron oxides can also be directly formed by dissolved $Fe^{2/3+}$ (Tsouris et al., 2001). For example, nano-sized magnetic iron oxides were prepared by $FeCl_3$ and then used for As adsorption, and the As-containing precipitate was easily separated under magnetic fields in a previous study (Lunge et al., 2014). In the process of in-situ preparation of magnetic iron oxides, a zero-valent iron plate was

electrochemically oxidized to produce magnetite in the As-containing solution system, and As was adsorbed on magnetite surfaces and removed from waters under a constant current (van Genuchten et al., 2020). In the electrocoagulation process of Fe(0) with a controlled constant-current density, the concentration of dissolved oxygen has a significant effect on the product phase and morphology of iron (hydr)oxides (Dubrawski et al., 2015). These processes require strict control of the current density, dissolved oxygen concentration and supporting electrolyte. Relative to constant (cell) voltage and current, constant potential can be utilized to better and more easily control the redox degree of iron in the electrocoagulation process (Liu et al., 2019). However, systematic studies are still needed to verify the possibility for the formation of magnetic iron oxides under constant potential and the corresponding adsorption and removal of As. In addition, there have been few reports on the removal of As from wastewater with magnetic iron oxides produced in situ by electrocoagulation (Bhateria and Singh, 2019).

In this work, zero-valent iron powder was used to treat simulated As-containing wastewater and actual mining wastewater by electrocoagulation under constant potential conditions. The magnetic iron oxides formed in the electrocoagulation process could facilitate the adsorption of As(V), and more importantly, help easy separation and recovery of As-containing precipitate under a magnetic field. The intermediates were characterized by X-ray diffractometion (XRD), Fourier transform infrared spectroscopy (FTIR), X-ray absorption spectroscopy (XAS) and field emission scanning electron microscopy (FESEM) to elucidate the electrocoagulation mechanism. The effects of potential, initial pH and supporting electrolyte on the formation process of magnetic iron oxides and removal ratio of As(V) were further investigated. The findings are expected to provide an efficient method for the treatment of As-containing wastewater.

2. Materials and methods

2.1 Electrochemical removal of As(V)

The working electrode was prepared by coating a mixture of zero-valent iron (ZVI) powder (MACKLIN) with particle size less than 150 μm and a polymeric binder (polyvinylidene fluoride, PVDF) on graphite paper (5.8 cm × 13 cm) with a mass ratio of 30:1. N-methyl-2-pyrrolidone (NMP) was added to PVDF as a dispersant with ultrasonic treatment. ZVI powder was mixed with NMP-dispersed PVDF polymeric binder, and then coated on graphite paper, which was dried in a vacuum oven at 40 ℃ for 6 h. The loading of ZVI powder was controlled to be 0.5 g with a coating electrode area of 3.8 cm × 5.8 cm.

Disodium hydrogen arsenate heptahydrate ($Na_2HAsO_4 \cdot 7H_2O$) was used to prepare simulated wastewater with 5 mg L^{-1} As(V) concentration. 0.1 mol L^{-1} $NaNO_3$ was used as the supporting electrolyte to control the ionic strength. The initial pH of the As(V)-containing solution was controlled at 7.0 by using 0.1 mol L^{-1} HNO_3 and 0.1 mol L^{-1} NaOH.

As-containing mining wastewater was sampled from a drain of nonferrous metal smeltery near a copper mine (E 114°55′47″, N 30°10′18″) in Daye City, Hubei Province, China on May 19, 2019. The wastewater was passed through a 0.45 μm filter membrane and then stored in a refrigerator at 4 ℃ for subsequent electrochemical treatment. The pH and conductivity of the wastewater were determined to be 8.06 and 1.42 mS cm^{-1}, respectively. The As(V) concentration and total organic carbon (TOC) were determined to be 5628.3 μg L^{-1} and 10.3 mg L^{-1}, respectively. The concentrations of Na^+, K^+, Ca^{2+} and Mn^{2+} were 622.7, 15.3, 125.4 and 0.6mg L^{-1}, and those of Cl^-, NO_3^- and SO_4^{2-} were 102.1, 85.1 and 532.1 mg L^{-1}, respectively. The concentrations of these ions

were different from those of the collected wastewater in our previous study (Liu et al., 2019). As(III), $Fe^{2/3+}$, Cu^{2+} and other possible heavy metal ions were not detected in the wastewater.

As(V) removal experiments were carried out using a three-electrode system with 600 mL As(V)-containing solution at room temperature. ZVI powder or blank graphite paper (5.8 cm × 13 cm) was used as the working electrode, while saturated calomel electrode (SCE) and graphite paper were used as reference electrode and counter electrode, respectively. The horizontal distance between the working electrode and the counter electrode was controlled at 7 cm. An electrochemical workstation (CHI660E, Shanghai Chenhua Instrument Co., Ltd.) was used to control the potential of the working electrode to range from –0.3 to 0.9 V (*vs.* SCE). The schematic diagram of the electrochemical system is shown in Fig. S1. In this work, the electrochemical potential values mentioned were expressed with respect to SCE. In the electrochemical reaction process, 10 mL solution was taken out at certain time intervals with a syringe and filtered by 0.2 μm filter membrane to determine the As(V) concentration in the filtrate. In order to avoid further oxidation or transformation of intermediates in the air, the solid products were immediately mixed with a drop of glycerol for XRD analysis. To elucidate the electrochemical mechanism for the removal of As(V) by ZVI powder, the control experiments of As(V) removal by ZVI electrode system at open circuit and blank graphite paper electrode system at 0.6 V were respectively carried out in open systems. To study the effect of supporting electrolyte on the removal ratio of As(V), 0.1 mol L^{-1} NaCl or Na_2SO_4 was used instead of $NaNO_3$, and 0.1 mol L^{-1} HCl or H_2SO_4 was used instead of HNO_3 for adjusting the initial pH of the corresponding reaction systems.

2.2. Solid-phase characterization and liquid-phase analysis

The crystal structures of the solid products were characterized by XRD (D8 ADVANCE diffractor with Cu Kα radiation). The characteristic functional groups of the solid products were analyzed by FTIR (Bruker VERTEX 70). FESEM (Hitachi SU8000) was used to characterize the micromorphology of the solid products. An atomic fluorescence spectrometer (AFS-8530, Beijing Haiguang Instrument Co., Ltd.) was used to determine the concentration of As(III). Before the determination of the concentration of total As [As(T)], As(V) was reduced to As(III) using ascorbic acid and thiourea. Then, the As(III) and As(T) concentrations were determined using 1.5%HCl−1.5%KBH_4 and 5%HCl−2%KBH_4 as the carrying fluid, respectively. The detailed calculation process of the As(V) removal ratio is shown with Eq. (S1) in the Supporting Information. The concentrations of K^+, Na^+, Ca^{2+}, Mn^{2+} and possible heavy metal ions in the wastewater were determined by atomic absorption spectrometry (Varian AAS240FS). XAS were measured on the 1W1B beamline at the Beijing Synchrotron Radiation Facility to characterize the species and proportion of the intermediates formed in the electrocoagulation system.

3. Results

3.1 Electrocoagulation of As(V)

In open environment systems, blank graphite paper and ZVI electrode were respectively used as the working electrode to remove As(V) from simulated wastewater. Fig. 1a shows the As(V) concentration in the solution with graphite paper and ZVI electrode as the working electrode at open circuit for 48 h, respectively. When ZVI electrode was used as the working electrode at open circuit, the As(V) concentration in the solution decreased from 5107.1 to 74.7 μg L^{-1} after 8 h, and after 48 h, the suspension showed an orange red color, with the As(V) concentration decreasing to

20.3 μg L^{-1} and a corresponding As(V) removal ratio of 99.6%. However, when graphite paper was used as the working electrode at open circuit, the As(V) concentration decreased from 5079.4 to 4870.6 μg L^{-1} after 48 h, with a corresponding As(V) removal ratio of only 4.1%. ZVI could be oxidized to iron (hydr)oxides likely due to the presence of dissolved oxygen. The newly formed iron (hydr)oxides could effectively adsorb the dissolved As(V), and the removal of As(V) through the inorganic adsorption of graphite paper could be neglected. Fig. 1b shows the As(V) concentration in the electrocoagulation system with graphite paper or ZVI powder as the working electrode at 0.6 V for 120 min. When 0.6 V was applied to the ZVI electrode for 120 min, the As(V) concentration first significantly decreased, followed by a slight increase, and then decreased again to reach equilibrium. The suspension showed an orange color within the first 20 min, then turned to brown at 40 min, and finally displayed a black color at 120 min (Fig. S2). The As(V) concentration decreased from 5127.5 to 57.9 μg L^{-1} within the first 20 min, followed by a gradual increase to 141.6 μg L^{-1} at 45 min, and then dropped to 26.8 μg L^{-1} at 120 min, with a corresponding As(V) removal ratio of 99.5%. These changes in the color of the suspension indicated variations of the chemical composition with the change of As(V) adsorption capacity. When ZVI was used as the working electrode, the As(V) removal ratio was significantly higher at 0.6 V than at open circuit. In order to further clarify the effect of ZVI oxidation on As(V) removal, blank graphite paper instead of ZVI was used as the working electrode at 0.6 V. As a result, the As(V) concentration decreased from 5237.9 to 4839.3 μg L^{-1} for 120 min (Fig. 1b), with a corresponding As(V) removal ratio of only 7.6%, which was significantly lower than the ratio when ZVI was used as the working electrode (99.5%). These results indicated that ZVI can further improve the removal ratio of As(V) in the electrocoagulation process.

The crystal structure and chemical composition of the solid products were characterized by XRD and FTIR in the electrocoagulation process. As shown in Fig. 2a and b, when ZVI powder was used as the working electrode at open circuit within 48 h, lepidocrocite was formed and its diffraction intensity increased with reaction time (Fig. 2a). In the FTIR spectra, the two absorption peaks at 3420 and 1654 cm^{-1} are assigned to the vibration of O–H in water, and the absorption peak at 3212 cm^{-1} is attributed to Fe–OH vibrations (Ristić et al., 2006). The bands at 1026 and 740 cm^{-1} are assigned to the characteristic absorption peaks of lepidocrocite (Antony et al., 2005), which is in agreement with the XRD results (Fig. 2b). When 0.6 V was applied, poorly crystalline iron oxides were first formed at the initial stage, and the crystallization degree increased with time, with the formation of maghemite and/or magnetite at 120 min (Fig. 2c). Magnetite and maghemite almost have the same diffraction peaks (Kim et al., 2012). The solid intermediates were further characterized by FTIR (Fig. 2d). The absorption peaks at 582 and 1630 and 3407 cm^{-1} are attributed to the Fe–O stretching vibration of magnetite, stretching vibrations and bending vibrations of adsorbed water and crystal water, respectively (Stoia et al., 2016). When electrocoagulation occurred at 60 min, an absorption peak appeared at 582 cm^{-1} with a strong asymmetric band due to the Fe–O stretching vibration, and the absorption peaks at 632, 700 and 809 cm^{-1} are assigned to Fe–O vibrations of maghemite (Ercuta and Chirita, 2013; Nazari et al., 2014). Therefore, a mixture of magnetite and maghemite was produced in the precipitate when ZVI was used for electrocoagulation at 0.6 V from 60 to 120 min. Fig. S3 presents the SEM images of the precipitate in the electrocoagulation system of As(V) when ZVI was used as the working electrode at open circuit for 48 h and at 0.6 V for 120 min. A large number of flake particles (Fig. S3a) of typical lepidocrocite were formed at open circuit (Hedenstedt et al., 2016), while spherical particles were

observed (Fig. S3b) at 0.6 V for 120 min, possibly due to the formation of magnetite and maghemite (Stoia et al., 2016).

In order to further clarify the generation and transformation process of iron (hydr)oxides in the electrocoagulation system, the precipitate formed at 0.6 V within 120 min was analyzed by linear combination fitting of EXAFS spectra at the Fe K edge (Fig. 3). As demonstrated in Table 1, a mixture of ferrihydrite and $GRCO_3$ was formed at 20 min, and magnetite was formed at 40 min, followed by the appearance of maghemite at 60 min. As shown in Fig. 3 and Table 1, the relative proportion of ferrihydrite and green rust decreased (from 81.5% and 18.5% to 1.1% and 7.8%, respectively) and that of magnetite and maghemite increased (from 0 to 73.7% and 17.4%, respectively) with time, suggesting the transformation of ferrihydrite and green rust to magnetite and/or maghemite, and magnetic iron oxides (mainly magnetite and maghemite) existed as the dominant components. These changes in chemical composition could also be reflected by magnetic experiments. The precipitate could be effectively adsorbed and separated at 120 min (Fig. S2).

The electrochemical oxidation of ZVI and the subsequent coagulation accelerated the removal of As(V). To clarify the possibility for the magnetic recovery of iron oxides, the inset photos in Fig. 1a and b show the color changes of the suspensions before and after magnetic adsorption with ZVI as the working electrode at open circuit for 48 h and at 0.6 V for 120 min, respectively. The iron oxides formed through the oxidation of dissolved oxygen at open circuit for 48 h could not be separated under a magnetic field. However, when 0.6 V was applied for 120 min, the finally formed black suspension could be rapidly clarified under a magnetic field, which could be attributed to the formation of magnetic iron oxides including magnetite and maghemite, despite the presence of small amounts of ferrihydrite and green rust in the precipitate.

3.2 Effect of potential

The increase in potential accelerated the electrochemical oxidation of ZVI, thus greatly improving the removal ratio of As(V) (Fig. 4a). The effect of applied potential on the As(V) removal was investigated in the electrocoagulation system with $NaNO_3$ as the supporting electrolyte and an initial pH of 7.0. When the potential was increased from −0.3 to 0.9 V, the As(V) removal ratio rose gradually within the first 5 min. The current also increased with increasing potential, suggesting an increase in the oxidation rate of ZVI (Fig. S4). When the potential was set at −0.3 and 0.9 V, the As(V) removal ratio was 11.0% and 65.6% at 5 min, and 99.1% and 99.0% at 120 min, respectively. These results indicated that an increase in potential could just enhance the As(V) removal ratio at the initial stage, and most of the As(V) could be removed within 120 min. Notably, the As(V) concentration first showed a rapid decrease, followed by a slight increase at about 60 min, and then decreased to reach equilibrium when the potential was controlled from 0 to 0.9 V. However, when the potential was controlled at −0.3 V, the As(V) concentration constantly decreased to reach equilibrium without further changes. The solid products in the suspension were further separated and characterized by XRD and FTIR (Fig. S5). As indicated by the XRD patterns, amorphous iron (hydr)oxides were formed at −0.3 V, while a mixture of magnetite and maghemite was formed at 0–0.9 V (Fig. S5a). The FTIR spectra were in agreement with the XRD results, and the Fe–O vibration peaks of magnetite and maghemite were not observed at −0.3 V (Fig. S5b). When electrocoagulation occurred with $NaNO_3$ as the supporting electrolyte at 0–0.9 V for 120 min, the precipitate could be easily separated and recovered by magnetic adsorption under a magnetic field; however, when the potential was set at −0.3 V, only part of the precipitate could be separated under

a magnetic field (Fig. S6), further indicating the formation of a mixture of magnetic iron oxides and poorly crystalline iron (hydr)oxides. In general, when electrocoagulation occurred at 0–0.9 V for 120 min, the precipitate could be quickly separated and recovered under a magnetic field with a slowdown of the increase in As(V) removal ratio with increasing potential. Therefore, the effects of initial pH and supporting electrolyte on As(V) removal ratio in the electrocoagulation process were studied at a potential of 0.6 V. Compared with previous reports (Kobya et al., 2011; Kobya et al., 2016), the electrode consumption represented by g ZVI per mg As ($C_{electrode/As}$) has certain advantages when the potential was controlled at 0.6 V, and calculation of the operating cost is described in Supporting Information (SI)

3.3 Effect of initial pH

Fig. 4b shows the concentrations of As(V) in the ZVI electrocoagulation system using $NaNO_3$ as the supporting electrolyte with different pH at 0.6 V. The As(V) removal ratio increased first followed by an obvious decrease with increasing initial pH in the first 15 min. When the initial pH was controlled at 3.0–9.0, the As(V) concentration significantly decreased at the initial stage, with a slight increase at about 40 min. When the initial pH was adjusted at 11.0, the As(V) removal ratio decreased. The As(V) concentration decreased from 5215.8 to 46.4 μg L^{-1} at initial pH 5.0, and from 5162.8 to 2742.0 μg L^{-1} at initial pH 11.0 in 15 min, which corresponded to an As(V) removal ratio of 99.1% and 46.9%, respectively, and at 120 min, the removal ratio reached almost 100% in both cases. The precipitates formed under different initial pH could be well separated under a magnetic field, which were further characterized by XRD and FTIR (Fig. S7). The results revealed that the precipitate in the suspension was a mixture of magnetite and maghemite when ZVI was

used as the working electrode at 0.6 V for 120 min under different initial pH.

3.4 Effect of supporting electrolyte

To investigate the effect of supporting electrolyte on As(V) removal, a ZVI electrocoagulation system was established at 0.6 V with the initial pH of 7.0, with Na_2SO_4 or NaCl being used as the supporting electrolyte instead of $NaNO_3$. As shown in Fig. 4c, no obvious difference was observed in the changing trend of As(V) concentration within 120 min. However, the As(V) removal ratio was calculated to be 97.8%, 99.6% and 64.8% at 10 min when 0.1 mol L^{-1} Na_2SO_4, NaCl and $NaNO_3$ were used as the supporting electrolyte, respectively, indicating that Na_2SO_4 and NaCl could better facilitate the adsorption of As(V) on the surface of intermediates than $NaNO_3$. When Na_2SO_4, NaCl and $NaNO_3$ were respectively used as the supporting electrolyte, different colors of suspensions and effects of magnetic separation were observed in the electrocoagulation process (Fig. S2). The suspension could not be well clarified when Na_2SO_4 or NaCl was used as the supporting electrolyte instead of $NaNO_3$, suggesting that different solid products might be formed. The solid products were then separated from the suspension and characterized by XRD and FTIR (Fig. S8). A mixture of green rust, $Fe(OH)_2$, magnetite, maghemite and δ−FeOOH was formed when Na_2SO_4 or NaCl was used as the supporting electrolyte (Fig. S8a and b), and the FTIR results further indicated that maghemite and magnetite were dominant in the solid products (Fig. S8c).

3.5 As(V) removal from mining wastewater

As-containing mining wastewater was collected near a mining and smelting plant. The wastewater was pretreated by bubbling of nitrogen gas to remove the dissolved CO_2, followed by

the addition of 0.1 mol L^{-1} $NaNO_3$ as the supporting electrolyte and adjustment of the pH to 3.0 using 0.1 mol L^{-1} HNO_3 and NaOH solution. When ZVI electrocoagulation was conducted at 0.6 V, the As(V) concentration showed a remarkable decrease from 5628.3 to 7.6 μg L^{-1} at 30 min, followed by a slight increase to 32.4 μg L^{-1} at 60 min, and then decreased to 3.6 μg L^{-1} at 24 h (Fig. 5a). The solid products could be easily separated by magnetic absorption as shown in the inset of Fig. 5a. Different from the changes of suspension color in the electrocoagulation of simulated As(V)-containing wastewater (Fig. S2), a brown suspension was formed for the actual arsenic-containing wastewater, which may be ascribed to different chemical compositions of the solid products. As shown in Fig. 5b, the XRD patterns indicated that the solid products were magnetite and/or maghemite, and the FTIR spectra further suggested that only maghemite was formed for the ZVI electrocoagulation of actual wastewater (Fig. 5c). The asymmetric absorption peak at 568 cm^{-1} is attributed to the vibration of γ Fe−O. The absorption bands at 468, 632, 695 and 1642 cm^{-1} are due to the characteristic absorption peaks of maghemite (Chakrabarti et al., 2004; Stoia et al., 2016).

4. Discussion

4.1 As(V) removal mechanism in electrocoagulation process

In the open circuit, the removal of 4.1% As can be ascribed to the adsorption of graphite paper. However, when 0.6 V was applied, the surface of working electrode should be positively charged, which improved the migration of As from the solution to the working electrode and the adsorption capacity of graphite paper for As. In addition, compared with the open circuit, the kinetic rate of As(V) removal was mainly affected by electrocoagulation at 0.6 V (Fig. S9). In the ZVI electrocoagulation process, the dissolved oxygen, pH and supporting electrolyte can affect the

formation and further transformation of iron oxides (Kobya et al., 2014). Metal Fe is electrochemically oxidized and dissolved with the release of Fe^{2+} or Fe^{3+}, and the electrochemically generated Fe^{2+} is easily oxidized to Fe^{3+} by dissolved oxygen, followed by the hydrolysis of Fe^{3+} to produce ferric hydroxides including ferrihydrite (Kobya et al., 2014; Mohora et al., 2018). Under a higher potential, water is decomposed with the release of H_2 gas and the generation of OH^- (Mohora et al., 2018). In the alkaline electrocoagulation solution with a low concentration of dissolved oxygen, green rust is the main hydrolysis product in the presence of CO_3^{2-}, SO_4^{2-} or Cl^- (Moreno et al., 2007). Green rust can be transformed to magnetite through dissolution–recrystallization under the absence of dissolved oxygen (Dubrawski et al., 2015; Perez et al., 2020). Ferrihydrite could also be transformed to magnetite in the presence of dissolved Fe(II) due to the adsorption and surface electron transfer from Fe(II) to Fe(III) oxides, which is accompanied by the dissolution–recrystallization process (Hansel et al., 2005). Magnetite could also be generated from the interaction between $Fe(OH)_2$ and $Fe(OH)_3$ (Kobya et al., 2011; Nidheesh and Singh, 2017).

In this work, the final pH values in the electrocoagulation system of ZVI and graphite paper electrodes at open circuit for 48 h and constant potential of 0.6 V for 120 min were not obviously different (Fig. S10), indicating that pH may not be the main factor influencing As(V) speciation and the phase of formed iron (hydr)oxides in this process. Ferrihydrite and green rust were formed as precipitates when electrocoagulation occurred at pH 8.0 after 20 min, and the concentration of dissolved oxygen was kept at a low value of 0.1 mg L^{-1} (Figs. S11 and S12). When electrocoagulation proceeded for over 40 min, the low concentration of dissolved oxygen facilitated the transformation of green rust to magnetite. Dissolved Fe(II) was continuously released during the

electrocoagulation process, which could accelerate the transformation of ferrihydrite to magnetite. During the reaction process, the pH was determined to be 9.0, and the hydrolysis of dissolved Fe(II) and Fe(III) occurred with the formation of magnetite (Kobya et al., 2011). Therefore, a mixture of magnetite, green rust and ferrihydrite was formed at the initial stage. At 60 min, maghemite was detected in the precipitate, which could be ascribed to the transformation of $Fe(OH)_3$ into maghemite in the solution (Kobya et al., 2011). The relative content of magnetite and maghemite showed continuous increases in the electrocoagulation process (Table 1), suggesting the continuous occurrence of the above possible transformation processes. Therefore, changes in the solution color could indicate the transformation between iron (hydr)oxides (Fig. S2). When green rust and ferrihydrite were formed in the suspension, the solution showed an orange color. Therefore, with increasing proportion of magnetite, the color of the solution would be deepened and change from orange to brown. With the electrocoagulation proceeding, the proportion of magnetite increased and that of green rust and ferrihydrite decreased, resulting in a final black color of the solution.

The transformation process could also be indicated by the changes in As(V) concentration. When ZVI electrocoagulation was conducted at 0.6 V and an initial pH of 7.0, the As(V) concentration remarkably decreased at first, suggesting the adsorption of As(V) in the initial stage, and showed a slight increase within 20–40 min, indicating the desorption of a small amount of As(V) from the precipitate, and then decreased after 45 min. There are many adsorption sites on the surface of iron (hydr)oxides, which can adsorb As(V) in the solution (Lakshmanan et al., 2010). Different iron (hydr)oxides exhibit various As adsorption capacities. With the transformation of amorphous iron oxide to more crystalline phases, the decrease in specific surface area and adsorption site density will increase the mobility of As (Dixit and Hering, 2003). In this work, green rust and ferrihydrite

were first formed, and then rapid As adsorption occurred with a remarkable decrease in As(V) concentration. At 40 min, magnetite was detected in the precipitate, and there were decreases in the proportion of green rust and ferrihydrite (Table 1 and Fig. 3). The formation of magnetite could be ascribed to the transformation of green rust and ferrihydrite in the solution (Dubrawski et al., 2015; Hansel et al., 2005). Compared with magnetite, green rust and ferrihydrite had a higher adsorption capacity for As, and thus the concentration of As in the solution increased within 20–40 min. After 45 min, the As(V) concentration decreased again with further As(V) removal, possibly due to increases in the amount of magnetite and maghemite with the proceeding of ZVI electrocoagulation. The removal mechanism of As(V) and the transformation between iron (hydr)oxides can be summarized by Eqs. (S2–S16).

The generation rate of Fe(II), dissolved oxygen concentration and supporting electrolyte significantly affect the formation process of magnetic iron oxides (Dubrawski et al., 2015). In this work, constant potential was used to control the oxidation degree of ZVI, and magnetic iron oxides formed in situ were used to remove As from wastewater. In addition, the electrocoagulation process is open to the air atmosphere without the need of controlling the atmosphere.

4.2 Effect of potential, initial pH and anions

The oxidation degree of ZVI was mainly controlled by the potential of the working electrode. The increase in potential gave rise to the removal ratio of As(V) due to the increase in the oxidation rate of ZVI (Fig. 4a). When the working electrode potential was increased from −0.3 to 0.9 V, the oxidation rate of ZVI increased as indicated by the cyclic voltammogram curves (Fig. S13). The decrease in dissolved oxygen concentration also suggested an increase in the oxidation rate of ZVI

with increasing working electrode potential (Fig. S14). In this work, the working electrode potential may play an important part in the oxidation of dissolved Fe(II). Therefore, the generation rate of ferrihydrite and green rust as well as the subsequent formation of magnetite and maghemite all decreased (Fig. S5) when a lower oxidation potential was applied to the working electrode. When the potential of ZVI working electrode was controlled at −0.3 V, only a small amount of maghemite was formed with a low degree of crystallization (Fig. S6), and the removal ratio of As(V) significantly decreased (Fig. 4a). Therefore, a proper higher oxidation potential should be applied for effective ZVI electrocoagulation.

The pH value affects the adsorption of As on iron (hydr)oxides, mainly because pH can affect the speciation of As and the surface charges on iron (hydr)oxides (Gallegos-Garcia et al., 2012; Kosmulski et al., 2003). In addition, the affinity of each As species to the surface of iron (hydr)oxides varies with changes in pH (Gallegos-Garcia et al., 2012). As(V) mainly exists in the form of both $H_2AsO_4^-$ and H_3AsO_4 when the solution pH is 3.0, while mainly in the form of $H_2AsO_4^-$ at pH 5.0 (Raven et al., 1998). Therefore, the removal ratio of As(V) at initial pH 5.0 was higher than that at initial pH 3.0 within the first 15 min (Fig. 4b). When the initial pH was adjusted to 11.0, As(V) mainly existed in the form of $HAsO_4^{2-}$, and the surface of iron (hydr)oxides was negatively charged, which may explain the obviously lower removal ratio of As(V) compared with that at pH 7.0 within the first 80 min (Dixit and Hering, 2003). When a higher voltage was applied in the electrocoagulation process, OH^- would be generated on the graphite paper electrode (Mohora et al., 2018), as indicated by Fig. S15. With increasing pH, there would be changes in As(V) species and the corresponding adsorption capacity of iron (hydr)oxides. The pH of the reaction system would change to about 9.0 at the later stage when the initial pH was adjusted at 3.0−11.0, possibly

because the release and consumption of OH^- reached equilibrium on the counter electrode. In the electrocoagulation process, abundant OH^- could facilitate the hydrolysis of $Fe^{2/3+}$ and flocculation of iron (hydr)oxides (Nidheesh and Singh, 2017); however, a too high concentration of OH^- would decrease the adsorption and the corresponding removal ratio of As(V). In this work, when the initial pH was adjusted at 5.0–7.0, a higher removal ratio of As(V) could be achieved, as indicated by the changes in As(V) concentration (Fig. 4b).

The supporting electrolyte affects the oxidation and dissolution of Fe and the further transformation of iron (hydr)oxides in the electrocoagulation process. When NaCl or Na_2SO_4 was used instead of $NaNO_3$ as the supporting electrolyte, the removal ratio of As(V) became slightly more significant (Fig. 4c) likely due to the formation of green rust, which could not be completely transformed to magnetite (Fig. S8a and b). Green rust particles have more abundant adsorption active sites than magnetite and maghemite, which can facilitate the adsorption of As(V) and enhance the corresponding removal ratio (Wang et al., 2010). Cl^- can diffuse into the oxide film of the ZVI electrode, preventing the formation of a passive film and promoting the oxidation dissolution of iron (Kim and Pyun, 1996; Zhao et al., 2018). SO_4^{2-} facilitates the formation and improves the chemical stability of green rust, though having no obvious influence on the formation of iron (hydr)oxides in the ZVI electrocoagulation process (Wan et al., 2011; Zhao et al., 2018). Previous research has been mostly focused on the effects of Cl^-, SO_4^{2-} and HCO_3^- on the formation of magnetic iron oxides (Dubrawski et al., 2015; van Genuchten et al., 2018). When NO_3^- was used as the supporting electrolyte, although the formation of passive film could not been completely blocked (Lakshmipathiraj et al., 2010) and the As(V) removal ratio was slightly lower than that when NaCl or Na_2SO_4 was used as the supporting electrolyte (Fig. 4c), magnetic iron oxides

including magnetite and maghemite could be easily formed and well separated, and the As(V) removal ratio could reach 99.5% at 120 min. Therefore, $NaNO_3$ might be a proper supporting electrolyte for As(V) removal in the ZVI electrocoagulation process.

4.3 As(V) removal from mining wastewater

For the actual wastewater, the total inorganic carbon (TIC) content and total organic carbon (TOC) were determined to be 8.1 and 10.3 mg L^{-1}, respectively. The organic matter has a negative impact on the removal of As due to its incomplete ionization in the solution (Khalil et al., 2018). Anions, in general, compete for the active sites on the surface of zero-valent iron, leading to negative interference with the As removal (Khalil et al., 2018). In addition, compared with the common ions in the wastewater, the presence of CO_3^{2-} will greatly affect the removal efficiency of As (Wen et al., 2014). When the CO_3^{2-} concentration is higher than 5 mg L^{-1}, the As removal ratio will apparently decrease, possibly due to the anodic passivation caused by the $FeCO_3$ precipitate generated by carbonate anions and the newly formed ferrous ions, which subsequently hinder the dissolution process of the ZVI electrode (Vasudevan et al., 2010). In our previous work, $CaCO_3$ precipitate was formed on the cathode surface due to Ca^{2+} enrichment and the subsequent reaction with CO_3^{2-} during the electrochemical adsorption of As(III, V) by manganese oxides (Liu et al., 2019). The green rust formed in the presence of CO_3^{2-} had the highest stability, followed by that formed in the presence of SO_4^{2-} and Cl^- (Zhao et al., 2018). The high stability of green rust is not conducive to the formation of magnetic oxides. Therefore, the pre-removal of water-soluble CO_2 may greatly enhance the removal ratio of As(V) and the formation of magnetic iron oxides. In this work, an appropriate concentration of $NaNO_3$ was added as the supporting electrolyte to increase the

conductivity, and the electrocoagulation system was bubbled with nitrogen gas and the pH was adjusted to 3.0 to reduce the effect of dissolved carbonate on the As(V) removal ratio and facilitate the formation of magnetic iron oxides. The highly efficient removal of As(V) and the formation of maghemite in the actual wastewater simplify the solid-liquid separation and reduce the treatment cost, providing a possible method for the treatment of industrial As-containing wastewaters in the future.

5. Conclusions

In this study, zero-valent iron (ZVI) powder was successfully applied to constant-potential electrocoagulation for the removal of As(V) from wastewater. Magnetic iron oxides including magnetite and maghemite were formed, which could facilitate the separation of precipitates from the suspension. Green rust and ferrihydrite were the intermediates for the electrochemical oxidation of ZVI to magnetic oxides in the electrocoagulation process. The As(V) removal ratio increased with increasing potential from −0.3 to 0.9 V; and with increasing initial pH from 3.0 to 11.0, the As(V) removal ratio increased first and then decreased, with the optimal pH at 5.0–7.0. When NaCl, Na_2SO_4 or $NaNO_3$ was used as the supporting electrolyte, the As(V) removal ratio followed the order of NaCl > Na_2SO_4 > $NaNO_3$. However, the presence of $NaNO_3$ was found to be more conducive to the formation of magnetic iron oxides and the subsequent separation of precipitates from the suspension. The removal efficiency of As(V) reached above 99.5% in the simulated and actual As-containing wastewaters. This work provides a feasible and effective method for the treatment of As-containing wastewaters and subsequent separation of precipitates.

Appendix A. Supplementary data

Supplementary data to this article can be found online.

Acknowledgements

The study was financially supported by the Project funded by National Natural Science Foundation of China (Nos. 42007127, 42077133 and 41877025), China Postdoctoral Science Foundation (No. BX20200144), the National Key Research and Development Program of China (No. 2020YFC1808503) and the Fundamental Research Funds for the Central Universities (Nos. 2662018JC055 and 2662015JQ002). S. L. S. thanks grant DE-FG02-86ER13622.A000 supported by the U.S. Department of Energy, Office of Basic Energy Sciences, Division of Chemical, Biological and Geological Sciences. The authors also thank Dr. Lirong Zheng at beamline 1W1B of Beijing Synchrotron Radiation Facility (BSRF) for the technical assistance with data collection and analysis, and Lihong Qin at Public Laboratory of Electron Microscope of Huazhong Agricultural University for helping with SEM analyses.

References

Alka, S.,Shahir, S.,Ibrahim, N.,Ndejiko, M.J.,Vo, D.-V.N., Abd Manan, F., 2020. Arsenic Removal Technologies And Future Trends: A Mini Review. J. Cleaner Prod. 278, 123805.

Antony, H.,Legrand, L.,Maréchal, L.,Perrin, S.,Dillmann, P., Chaussé, A., 2005. Study of lepidocrocite γ-FeOOH electrochemical reduction in neutral and slightly alkaline solutions at 25°C. Electrochim. Acta 51, 745–753.

Aredes, S.,Klein, B., Pawlik, M., 2013. The removal of arsenic from water using natural iron oxide

minerals. J. Cleaner Prod. 60, 71−76.

Bhateria, R., Singh, R., 2019. A review on nanotechnological application of magnetic iron oxides for heavy metal removal. J. Water Process Eng. 31, 100845.

Chakrabarti, S.,Ganguli, D., Chaudhuri, S., 2004. Optical properties of γ-Fe_2O_3 nanoparticles dispersed on sol–gel silica spheres. Physica E 24, 333−342.

Choong, T.S.,Chuah, T.,Robiah, Y.,Koay, F.G., Azni, I., 2007. Arsenic toxicity, health hazards and removal techniques from water: an overview. Desalination 217, 139−166.

Chowdhury, U.K.,Biswas, B.K.,Chowdhury, T.R.,Samanta, G.,Mandal, B.K.,Basu, G.C.,Chanda, C.R.,Lodh, D.,Saha, K.C., Mukherjee, S.K., 2000. Groundwater arsenic contamination in Bangladesh and West Bengal, India. Environ. Health Perspect. 108, 393−397.

Dixit, S., Hering, J.G., 2003. Comparison of arsenic(V) and arsenic(III) sorption onto iron oxide minerals: implications for arsenic mobility. Environ. Sci. Technol. 37, 4182−4189.

Dubrawski, K.L.,van Genuchten, C.M.,Delaire, C.,Amrose, S.E.,Gadgil, A.J., Mohseni, M., 2015. Production and transformation of mixed-valent nanoparticles generated by Fe(0) electrocoagulation. Environ. Sci. Technol. 49, 2171−2179.

Edition, F., 2011. Guidelines for drinking-water quality. WHO chronicle 38, 104−108.

Eljamal, O.,Sasaki, K., Hirajima, T., 2011. Numerical simulation for reactive solute transport of arsenic in permeable reactive barrier column including zero-valent iron. Appl. Math. Modell. 35, 5198−5207.

Eljamal, O.,Sasaki, K.,Tsuruyama, S., Hirajima, T., 2011. Kinetic model of arsenic sorption onto zero-valent iron (ZVI). Water Qual. Exposure Health 2, 125−132.

Eljamal, O.,Sasaki, K., Hirajima, T., 2013. Sorption kinetic of arsenate as water contaminant on

zero valent iron. J. Water Resour. Prot. 5, 563−567.

Ercuta, A., Chirita, M., 2013. Highly crystalline porous magnetite and vacancy-ordered maghemite microcrystals of rhombohedral habit. J. Cryst. Growth 380, 182−186.

Fu, F.,Dionysiou, D.D., Liu, H., 2014. The use of zero-valent iron for groundwater remediation and wastewater treatment: a review. J. Hazard. Mater. 267, 194–205.

Gallegos-Garcia, M.,Ramírez-Muñiz, K., Song, S., 2012. Arsenic removal from water by adsorption using iron oxide minerals as adsorbents: a review. Miner. Process. Extr. Metall. Rev. 33, 301−315.

Gong, Z.,Lu, X.,Ma, M.,Watt, C., Le, X.C., 2002. Arsenic speciation analysis. Talanta 58, 77−96.

Hakizimana, J.N.,Gourich, B.,Chafi, M.,Stiriba, Y.,Vial, C.,Drogui, P., Naja, J., 2017. Electrocoagulation process in water treatment: A review of electrocoagulation modeling approaches. Desalination 404, 1−21.

Hansel, C.M.,Benner, S.G., Fendorf, S., 2005. Competing Fe(II)-induced mineralization pathways of ferrihydrite. Environ. Sci. Technol. 39, 7147−7153.

He, R.,Peng, Z.,Lyu, H.,Huang, H.,Nan, Q., Tang, J., 2018. Synthesis and characterization of an iron-impregnated biochar for aqueous arsenic removal. Sci. Total Environ. 612, 1177−1186.

Hedenstedt, K.,Gomes, A.S.,Busch, M., Ahlberg, E., 2016. Study of hypochlorite reduction related to the sodium chlorate process. Electrocatalysis 7, 326−335.

Khalil, A.M.,Eljamal, O.,Amen, T.W.,Sugihara, Y., Matsunaga, N., 2018. Scrutiny of interference effect of ions and organic matters on water treatment using supported nanoscale zero-valent iron. Environ. Earth Sci. 77, 1−13.

Kim, J.-D., Pyun, S.-I., 1996. The effects of applied potential and chloride ion on the repassivation

kinetics of pure iron. Corros. Sci. 38, 1093−1102.

Kim, W.,Suh, C.-Y.,Cho, S.-W.,Roh, K.-M.,Kwon, H.,Song, K., Shon, I.-J., 2012. A new method for the identification and quantification of magnetite–maghemite mixture using conventional X-ray diffraction technique. Talanta 94, 348−352.

Kobya, M.,Gebologlu, U.,Ulu, F.,Oncel, S., Demirbas, E., 2011. Removal of arsenic from drinking water by the electrocoagulation using Fe and Al electrodes. Electrochim. Acta 56, 5060−5070.

Kobya, M.,Ulu, F.,Gebologlu, U.,Demirbas, E., Oncel, M.S., 2011. Treatment of potable water containing low concentration of arsenic with electrocoagulation: Different connection modes and Fe–Al electrodes. Sep. Purif. Technol. 77, 283−293.

Kobya, M.,Akyol, A.,Demirbas, E., Oncel, M., 2014. Removal of arsenic from drinking water by batch and continuous electrocoagulation processes using hybrid Al - Fe plate electrodes. Environ. Prog. Sustainable Energy 33, 131−140.

Kobya, M.,Demirbas, E., Ulu, F., 2016. Evaluation of operating parameters with respect to charge loading on the removal efficiency of arsenic from potable water by electrocoagulation. J. Environ. Chem. Eng. 4, 1484−1494.

Kobya, M.,Soltani, R.D.C.,Omwene, P.I., Khataee, A., 2020. A review on decontamination of arsenic-contained water by electrocoagulation: Reactor configurations and operating cost along with removal mechanisms. Environ. Technol. Innovation 17, 100519.

Kosmulski, M.,Maczka, E.,Jartych, E., Rosenholm, J.B., 2003. Synthesis and characterization of goethite and goethite–hematite composite: experimental study and literature survey. Adv. Colloid Interface Sci. 103, 57−76.

Lacasa, E.,Sáez, C.,Cañizares, P.,Fernández, F.J., Rodrigo, M.A., 2013. Arsenic removal from high-

arsenic water sources by coagulation and electrocoagulation. Sep. Sci. Technol. 48, 508–514.

Lakshmanan, D.,Clifford, D.A., Samanta, G., 2009. Ferrous and ferric ion generation during iron electrocoagulation. Environ. Sci. Technol. 43, 3853–3859.

Lakshmanan, D.,Clifford, D.A., Samanta, G., 2010. Comparative study of arsenic removal by iron using electrocoagulation and chemical coagulation. Water Res. 44, 5641–5652.

Lakshmipathiraj, P.,Prabhakar, S., Raju, G.B., 2010. Studies on the electrochemical decontamination of wastewater containing arsenic. Sep. Purif. Technol. 73, 114–121.

Liu, L.,Tan, W.,Suib, S.L.,Qiu, G.,Zheng, L., Su, S., 2019. Enhanced adsorption removal of arsenic from mining wastewater using birnessite under electrochemical redox reactions. Chem. Eng. J. 375, 122051.

Lunge, S.,Singh, S., Sinha, A., 2014. Magnetic iron oxide (Fe_3O_4) nanoparticles from tea waste for arsenic removal. J. Magn. Magn. Mater. 356, 21–31.

Mohora, E.,Rončević, S.,Agbaba, J.,Zrnić, K.,Tubić, A., Dalmacija, B., 2018. Arsenic removal from groundwater by horizontal-flow continuous electrocoagulation (EC) as a standalone process. J. Environ. Chem. Eng. 6, 512–519.

Mondal, P.,Majumder, C., Mohanty, B., 2006. Laboratory based approaches for arsenic remediation from contaminated water: recent developments. J. Hazard. Mater. 137, 464–479.

Mondal, P.,Bhowmick, S.,Chatterjee, D.,Figoli, A., Van der Bruggen, B., 2013. Remediation of inorganic arsenic in groundwater for safe water supply: a critical assessment of technological solutions. Chemosphere 92, 157–170.

Moreno, H.A.,Cocke, D.L.,Gomes, J.A.,Morkovsky, P.,Parga, J.,Peterson, E., Garcia, C., 2007. Electrochemical generation of green rust using electrocoagulation. ECS Trans. 3, 67.

Nazari, M.,Ghasemi, N.,Maddah, H., Motlagh, M.M., 2014. Synthesis and characterization of maghemite nanopowders by chemical precipitation method. J. Nanostruct. Chem. 4, 99.

Nidheesh, P.V., Singh, T.S.A., 2017. Arsenic removal by electrocoagulation process: recent trends and removal mechanism. Chemosphere 181, 418−432.

Perez, J.P.H.,Schiefler, A.A.,Rubio, S.N.,Reischer, M.,Overheu, N.D.,Benning, L.G., Tobler, D.J., 2020. Arsenic removal from natural groundwater using 'green rust': Solid phase stability and contaminant fate. J. Hazard. Mater. 401, 123327.

Raven, K.P.,Jain, A., Loeppert, R.H., 1998. Arsenite and arsenate adsorption on ferrihydrite: kinetics, equilibrium, and adsorption envelopes. Environ. Sci. Technol. 32, 344−349.

Ristić, M.,Musić, S., Godec, M., 2006. Properties of γ-FeOOH, α-FeOOH and α-Fe_2O_3 particles precipitated by hydrolysis of Fe^{3+} ions in perchlorate containing aqueous solutions. J. Alloys Compd. 417, 292−299.

Siddiqui, S.I., Chaudhry, S.A., 2017. Iron oxide and its modified forms as an adsorbent for arsenic removal: A comprehensive recent advancement. Process Saf. Environ. Prot. 111, 592−626.

Singh, R.,Singh, S.,Parihar, P.,Singh, V.P., Prasad, S.M., 2015. Arsenic contamination, consequences and remediation techniques: a review. Ecotoxicol. Environ. Saf. 112, 247−270.

Song, P.,Yang, Z.,Zeng, G.,Yang, X.,Xu, H.,Wang, L.,Xu, R.,Xiong, W., Ahmad, K., 2017. Electrocoagulation treatment of arsenic in wastewaters: A comprehensive review. Chem. Eng. J. 317, 707−725.

Stoia, M.,Istratie, R., Păcurariu, C., 2016. Investigation of magnetite nanoparticles stability in air by thermal analysis and FTIR spectroscopy. J. Therm. Anal. Calorim. 125, 1185−1198.

Su, C., 2017. Environmental implications and applications of engineered nanoscale magnetite and

its hybrid nanocomposites: A review of recent literature. J. Hazard. Mater. 322, 48−84.

Thakur, L.S.,Goyal, H., Mondal, P., 2019. Simultaneous removal of arsenic and fluoride from synthetic solution through continuous electrocoagulation: Operating cost and sludge utilization. J. Environ. Chem. Eng. 7, 102829.

Tsouris, C.,DePaoli, D.,Shor, J.,Hu, M.-C., Ying, T.-Y., 2001. Electrocoagulation for magnetic seeding of colloidal particles. Colloids Surf., A 177, 223−233.

Tuutijärvi, T.,Lu, J.,Sillanpää, M., Chen, G., 2009. As(V) adsorption on maghemite nanoparticles. J. Hazard. Mater. 166, 1415−1420.

Ungureanu, G.,Santos, S.,Boaventura, R., Botelho, C., 2015. Arsenic and antimony in water and wastewater: overview of removal techniques with special reference to latest advances in adsorption. J. Environ. Manage. 151, 326−342.

van Genuchten, C.,Behrends, T.,Kraal, P.,Stipp, S.L., Dideriksen, K., 2018. Controls on the formation of Fe(II, III) (hydr)oxides by Fe(0) electrolysis. Electrochim. Acta 286, 324−338.

van Genuchten, C.M.,Behrends, T.,Stipp, S., Dideriksen, K., 2020. Achieving arsenic concentrations of < 1 μg/L by Fe(0) electrolysis: The exceptional performance of magnetite. Water Res. 168, 115170.

Vasudevan, S.,Lakshmi, J., Sozhan, G., 2010. Studies relating to removal of arsenate by electrochemical coagulation: optimization, kinetics, coagulant characterization. Sep. Sci. Technol. 45, 1313−1325.

Wan, W.,Pepping, T.J.,Banerji, T.,Chaudhari, S., Giammar, D.E., 2011. Effects of water chemistry on arsenic removal from drinking water by electrocoagulation. Water Res. 45, 384−392.

Wang, Y.,Morin, G.,Ona-Nguema, G.,Juillot, F.,Guyot, F.,Calas, G., Brown Jr, G.E., 2010. Evidence

for different surface speciation of arsenite and arsenate on green rust: an EXAFS and XANES study. Environ. Sci. Technol. 44, 109−115.

Wen, Z.,Zhang, Y., Dai, C., 2014. Removal of phosphate from aqueous solution using nanoscale zerovalent iron (nZVI). Colloids Surf., A 457, 433−440.

Zhang, L.,Qin, X.,Tang, J.,Liu, W., Yang, H., 2017. Review of arsenic geochemical characteristics and its significance on arsenic pollution studies in karst groundwater, Southwest China. Appl. Geochem. 77, 80−88.

Zhao, L.,Chen, Y.,Feng, Y., Wu, D., 2018. Oxidation of acetaminophen by Green rust coupled with Cu(II) via dioxygen activation: The role of various interlayer anions (CO_3^{2-}, SO_4^{2-}, Cl^-). Chem. Eng. J. 350, 930−938.

Table:

Table 1 Fitting results of Fe K Edge EXAFS spectra of the precipitate in electrochemical system of As(V) and $NaNO_3$ (0.1 mol L^{-1}) at 0.6 V for 120 min with initial pH 7.0.

Time	Ferrihydrite (%)	$GRCO_3$ (%)	Magnetite (%)	Maghemite (%)	R-factor
20 min	81.5	18.5	0.0	0.0	0.0219
40 min	70.3	22.8	6.9	0.0	0.0080
60 min	65.9	7.3	24.4	2.5	0.0154
80 min	43.6	10.0	38.1	8.3	0.0164
120 min	1.1	7.8	73.7	17.4	0.0059

Figure captions:

Fig. 1. Concentrations of As(V) in the electrocoagulation system of ZVI and graphite paper electrodes at open circuit for 48 h (a) and constant potential of 0.6 V for 120 min (b). The inset photos in (a) and (b) are respectively the photos of the suspension before and after magnetic adsorption under different conditions.

Fig. 2. XRD patterns and FTIR spectra of the precipitate in the electrocoagulation system of As(V) using ZVI electrode at open circuit for 48 h (a, b) and at 0.6 V for 120 min (c, d).

Fig. 3. Fe K edge EXAFS spectra (solid lines) and the corresponding linear combination fitting (gray dashed lines) of the precipitate in the electrocoagulation system of As(V) using ZVI electrode with initial pH 7.0 at 0.6 V for 120 min.

Fig. 4. Concentrations of As(V) in the electrocoagulation system using ZVI electrode under different conditions: (a) 0.1 mol L^{-1} $NaNO_3$, −0.3 to 0.9 V, initial pH 7.0; (b) 0.1 mol L^{-1} $NaNO_3$, 0.6 V, initial pH 3.0−11.0; (c) 0.1 mol L^{-1} $NaNO_3$, Na_2SO_4 and NaCl, 0.6 V, initial pH 7.0.

Fig. 5. Concentration of As(V) (a) in the actual wastewater and the XRD pattern (b) and FTIR spectrum (c) of the corresponding precipitate using electrocoagulation by ZVI electrode at 0.6 V for 24 h, and the inset photos in (a) are the photos of the suspension before and after magnetic adsorption.

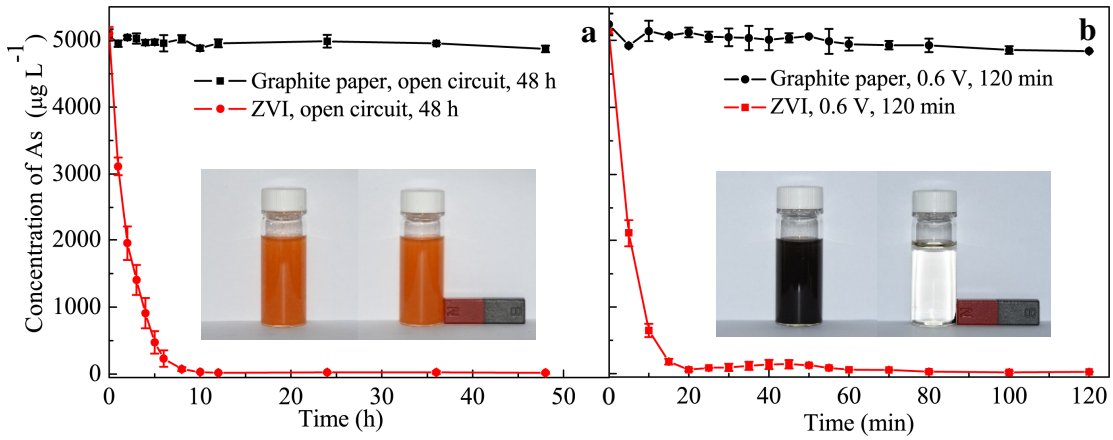

Fig. 1. Concentrations of As(V) in the electrocoagulation system of ZVI and graphite paper electrodes at open circuit for 48 h (a) and constant potential of 0.6 V for 120 min (b). The inset photos in (a) and (b) are respectively the photos of the suspension before and after magnetic adsorption under different conditions.

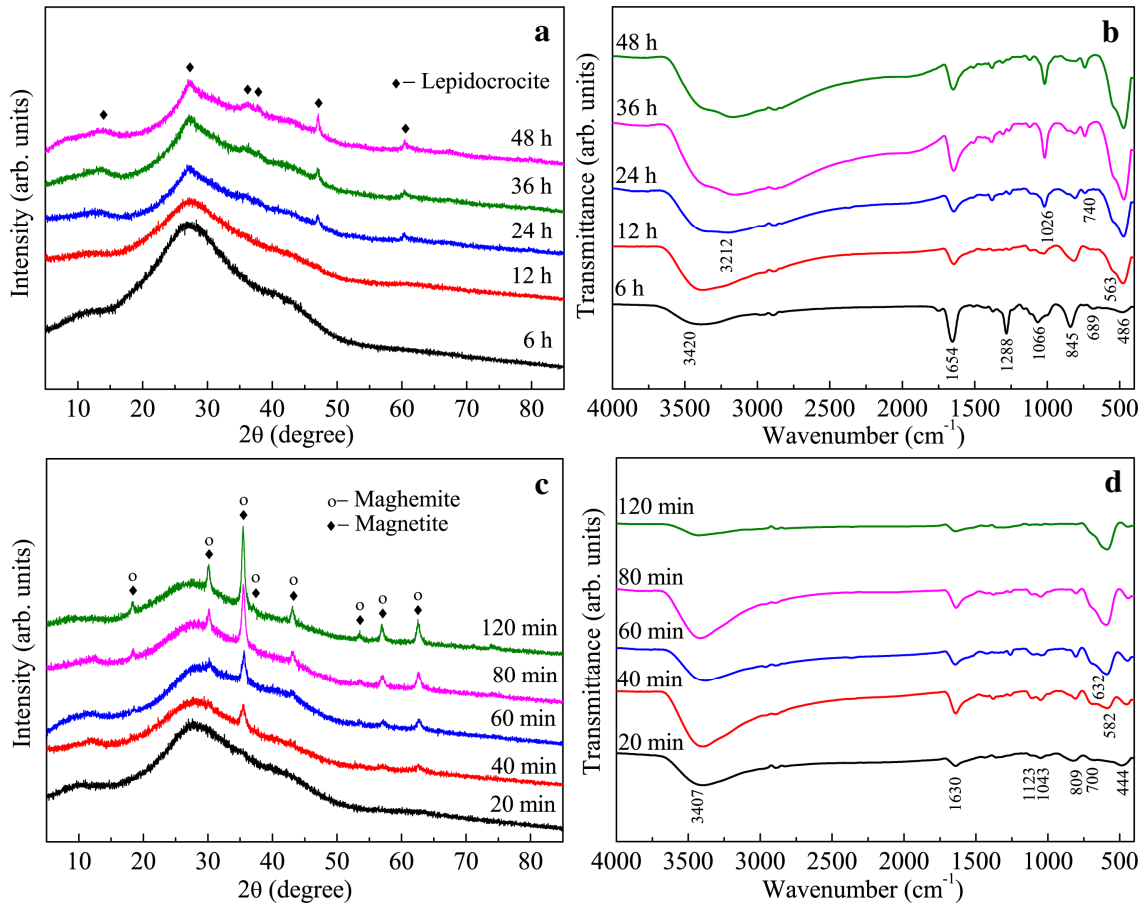

Fig. 2. XRD patterns and FTIR spectra of the precipitate in the electrocoagulation system of As(V) using ZVI electrode at open circuit for 48 h (a, b) and at 0.6 V for 120 min (c, d).

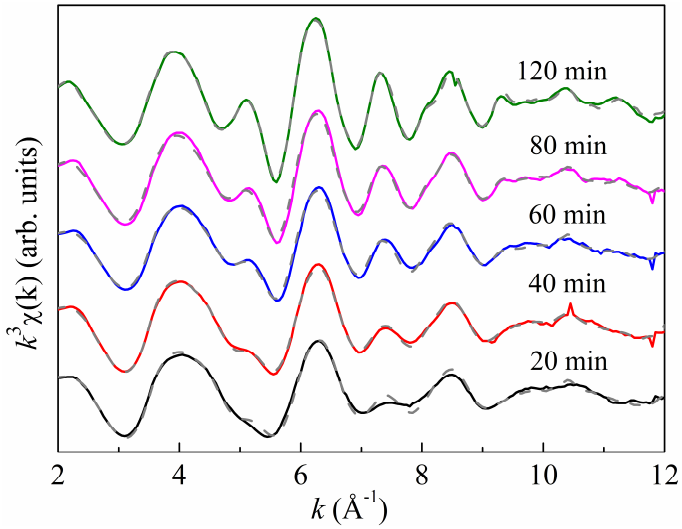

Fig. 3. Fe K edge EXAFS spectra (solid lines) and the corresponding linear combination fitting (gray dashed lines) of the precipitate in the electrocoagulation system of As(V) using ZVI electrode with initial pH 7.0 at 0.6 V for 120 min.

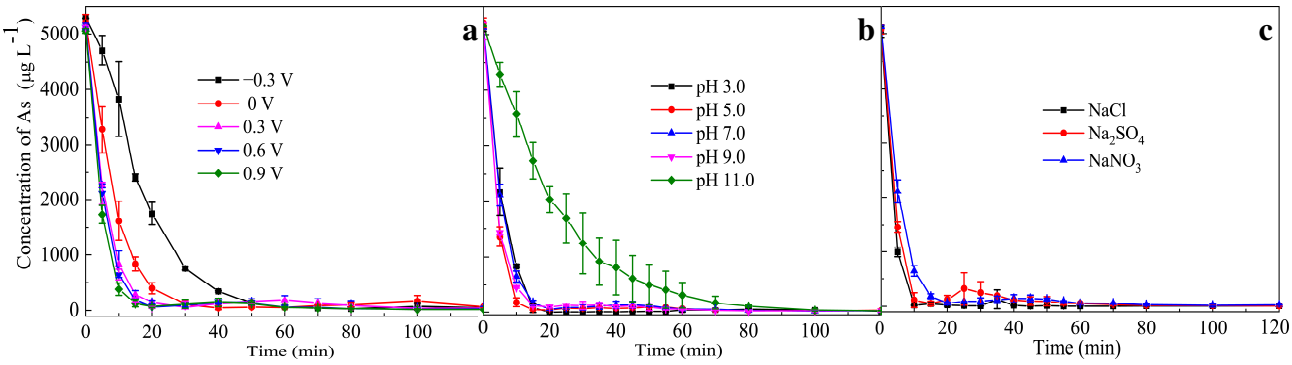

Fig. 4. Concentrations of As(V) in the electrocoagulation system using ZVI electrode under different conditions: (a) 0.1 mol L^{-1} $NaNO_3$, –0.3 to 0.9 V, initial pH 7.0; (b) 0.1 mol L^{-1} $NaNO_3$, 0.6 V, initial pH 3.0–11.0; (c) 0.1 mol L^{-1} $NaNO_3$, Na_2SO_4 and NaCl, 0.6 V, initial pH 7.0.

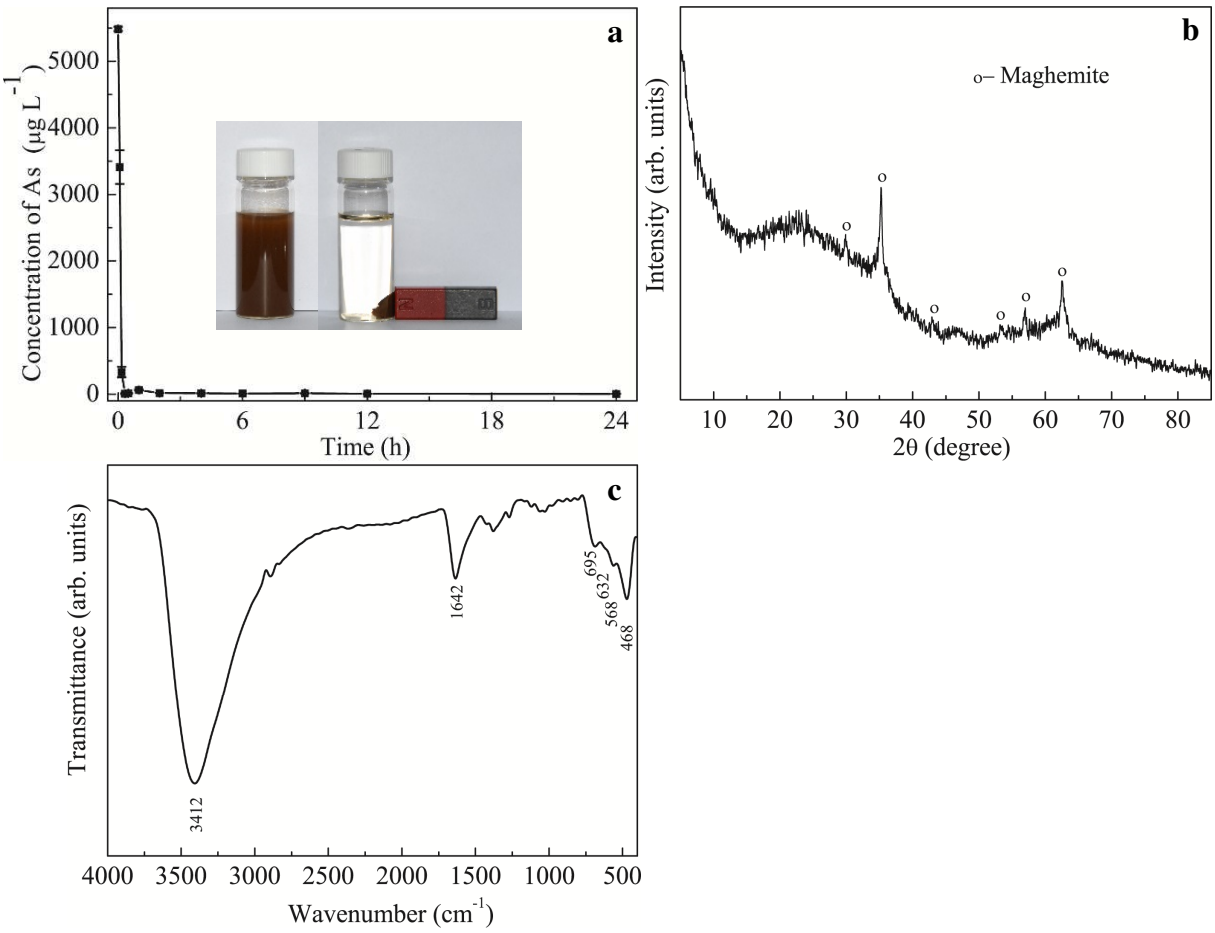

Fig. 5. Concentration of As(V) (a) in the actual wastewater and the XRD pattern (b) and FTIR spectrum (c) of the corresponding precipitate using electrocoagulation by ZVI electrode at 0.6 V for 24 h, and the inset photos in (a) are the photos of the suspension before and after magnetic adsorption.

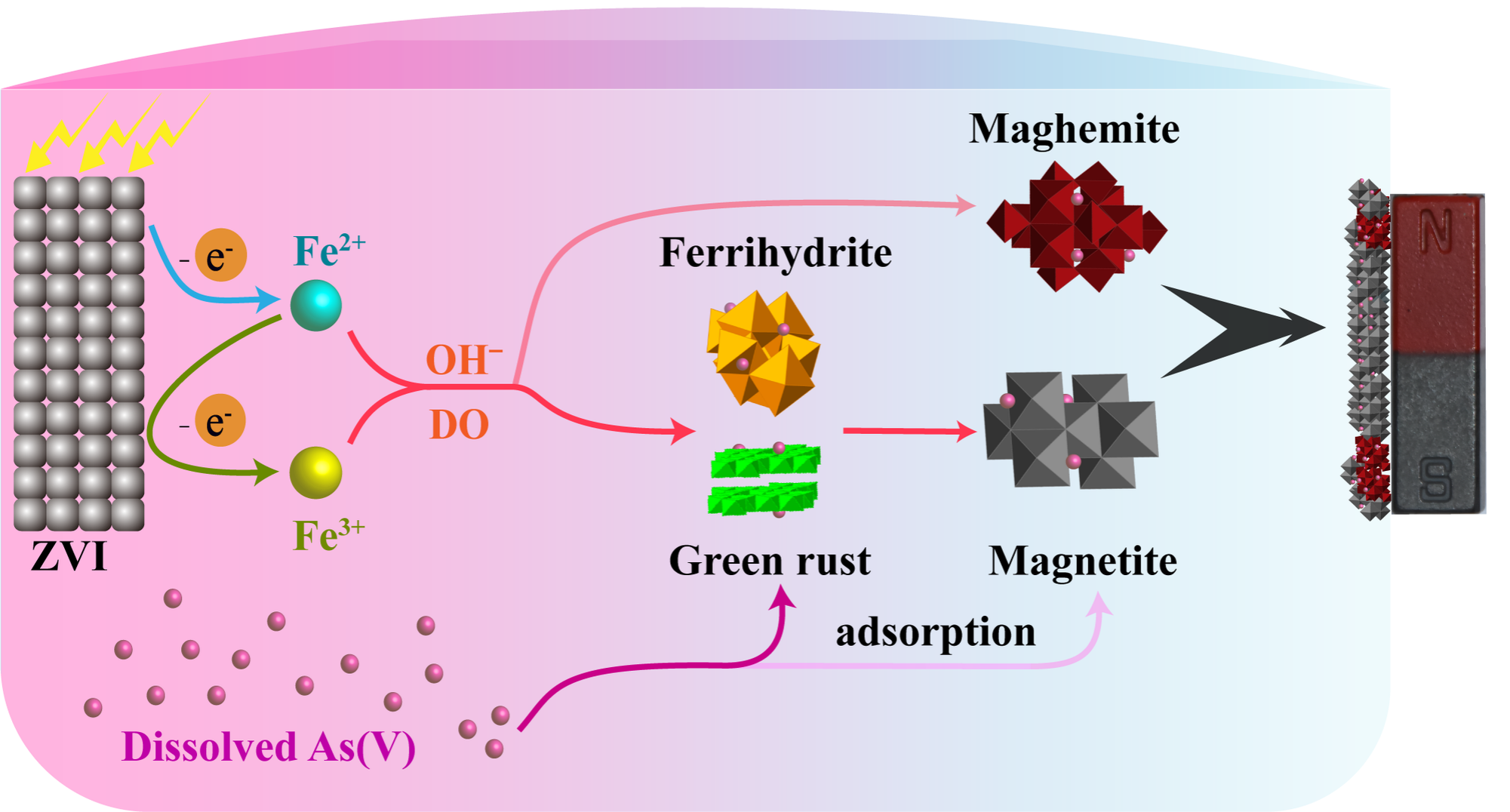
Maghemite
Ferrihydrite
- e⁻
- e⁻
Fe2+
Fe3+
OH⁻
DO
ZVI
Green rust
Magnetite
adsorption
Dissolved As(V)
N
S